IOP Publishing Plasma Sources Science and Technology
Plasma Sources Sci. Technol. **29** (2020) 105012 (11pp) https://doi.org/10.1088/1361-6595/abb7be

Time and space resolved diagnostics for plasma thermal-chemical instability of fuel oxidation in nanosecond plasma discharges

Aric C Rousso[1,2,*], Benjamin M Goldberg[1,3], Timothy Y Chen[1], Shuqun Wu[1,4], Arthur Dogariu[1], Richard B Miles[1,5], Egemen Kolemen[1,6] and Yiguang Ju[1]

[1] Department of Mechanical and Aerospace Engineering, Princeton University, Princeton, NJ 08544, United States of America
[2] Currently with Lawrence Livermore National Laboratory, Livermore, CA 94550, United States of America
[3] Currently with the Combustion Research Facility, Sandia National Laboratories, Livermore, California 94551, United States of America
[4] College of Automation Engineering, Nanjing University of Aeronautics and Astronautics, Nanjing, Jiangsu 210016, People's Republic of China
[5] Department of Aerospace Engineering, Texas A & M University, College Station, TX 77843, United States of America
[6] Princeton Plasma Physics Laboratory, Princeton, NJ 08544, United States of America

E-mail: acrousso@gmail.com

Received 2 May 2020, revised 2 September 2020
Accepted for publication 11 September 2020
Published 29 October 2020

Abstract

An instability in a nanosecond pulsed dielectric barrier discharge plasma occurring in methane–oxygen–argon mixtures is experimentally observed and measured by 1D time-resolved *in situ* electric field measurements. This instability, which seems to be created by the positive feedback between plasma kinetics and plasma-assisted low temperature fuel oxidation, is studied using electric field induced second harmonic generation and direct ICCD imaging. The rapid formation of streamers from an originally uniform discharge appears to be caused by the chemical kinetics of plasma-assisted low temperature methane oxidation, which may be resulting in a new type of plasma instability: a thermal-chemical instability. The results also revealed that the occurrence of this possible thermal-chemical instability in a reactive flow drastically changes the plasma properties by forming multiple secondary discharges and possibly leads to micron-sized non-uniform electric distributions. Single shot uncalibrated measurements of the electric field of the micron sized streamers appears to show much greater strengths than the average electric field. Furthermore, one-dimensional data analysis shows the positive feedback loop between the streamers and the low temperature plasma assisted oxidation chemistry in the plasma thermal-chemical instability. The present finding advances the understanding plasma instability growth and provides a new way to control plasma uniformity in plasma-assisted combustion and plasma fuel reforming.

Keywords: electric field measurements, second harmonic generation, plasma assisted oxidation, nanosecond pulsed DBD plasma discharge, E-FISH

S Supplementary material for this article is available online

(Some figures may appear in colour only in the online journal)

* Author to whom any correspondence should be addressed.

1. Introduction

As the world transitions to low carbon energy, the increasing utilization of renewable energy provides a unique opportunity to convert fossil energy into low carbon chemicals [1] and materials [2–4] using non-equilibrium plasmas. In addition, to develop advanced lean burn engines with low carbon emissions, it is critical to control plasma properties to achieve efficient ignition [1–5]. For these applications, diffuse, volumetric, nonthermal discharges are needed to meet high chemical reactivity, low power consumption, and high efficiency [5–7]. Therefore, it is of great importance to understand the mechanism of plasma instabilities in a chemically reactive flow.

Several mechanisms of plasma instabilities such as physically driven plasma destabilization [8, 9], the secondary-electron-emission instability [10], universal instability with a magnetic field in an inhomogeneous plasma [11], and plasma thermal instability via Joule heating [12] have been reported. For a plasma thermal instability, as shown in figure 1, the positive feedback between the change in electron number density (n_e), Joule heating (jE, a product of current j and electric field E), temperature (T), gas number density (N), and the reduced electric field is as follows: the electron number density locally increases leading to an increase in Joule heating which raises the temperature and causes the gas number density to decrease. This decrease in gas number density results in an increased reduced electric field, which further increases the electron number density and grows the instability ($n_e\uparrow \rightarrow jE\uparrow \rightarrow T\uparrow \rightarrow N\downarrow \rightarrow E/N\uparrow \rightarrow n_e\uparrow$). The plasma thermal instability mechanism has been studied in noble gases and air [12–15]. Physically, it has also been found that plasma destabilization can occur based on the strength of local electric field through changing the discharge gap or applied voltage [8] or through changing the rate of voltage rise and the peak applied voltage [9]. However, the mechanism of plasma instabilities during discharges that occur in chemically reactive and combustible mixtures is not well-understood. As shown in figure 1, in a chemically reactive flow, the elementary chemical reactions in the process such as the electron impact fuel dissociation, electron attachment affected by oxygen consumption and water formation, species changes in the plasma-assisted reaction process, and plasma-assisted low and high temperature fuel oxidation [16, 17] also contribute to either negative or positive feedback of the change of electron number density. In fact, in an early experiment of energy coupling to the plasma of repetitive nanosecond pulse discharges in a reactive ethylene/air mixture [18], it was clearly shown that the plasma instability of a reactive mixture developed much faster than that in air. The mechanism for plasma instability in this reactive mixture, however, was not investigated.

To understand plasma instability in a reactive flow, several studies have explored methods to eliminate the instability [14, 19–21] through the use of different bath gases. The results showed that there is a profound effect on the uniformity of the plasma due to changes in thermal and mass diffusivity. It has also been shown that the plasma instability

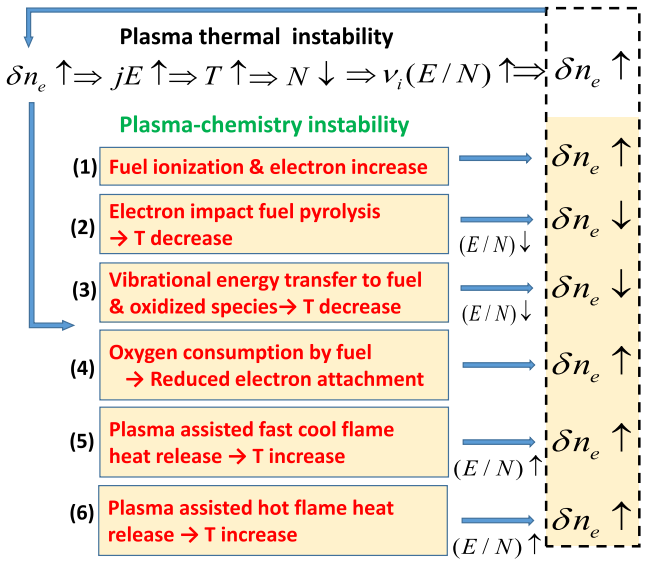

Figure 1. Schematic of the mechanisms for plasma thermal instability and plasma chemistry instability.

can be mitigated by either preheating the gas or raising the mixture temperature [18–20]. While these experimental studies provide useful observations of plasma instability, the cause of the thermal chemical instability formation in a chemically reactive flow remains unclear. Recently, with a hypothesis of plasma chemistry instability, the authors numerically studied the contraction process in a fuel-lean $H_2/O_2/N_2$ mixture with a simple plasma combustion kinetic model [22]. The results showed clearly that there is a plasma thermal-chemical instability and the elementary reactions of combustion kinetics can either decelerate or accelerate the occurrence of said instability. However, to date, few detailed experimental diagnostics have been carried to understand the physical process of plasma chemical instability formation.

Significant progress has been made in the development of new techniques to quantify the dynamics and properties of non-equilibrium plasmas. For example, the electric field measurements using electric field induced second harmonic generation (E-FISH) has made it possible to measure time-dependent local electric fields in a non-equilibrium plasma with any gaseous species [6, 23–26]. Briefly, second harmonic generation is impossible in a centrosymmetric medium. However, in the presence of an external electric field, a net dipole is induced in the gaseous species, destroying the inversion symmetry and allowing for a coherent buildup of radiation at the second harmonic frequency of an intense laser source. The effect was first discovered in the 1960's and 70's and has mostly been used to measure the hyperpolarizability of different molecules [27, 28]. The method was first demonstrated as an effective technique for electric field measurements in 2017 [23]. Since then, several groups around the world have adopted the method using femto-, pico-, and nanosecond laser pulses for measurements in a variety of plasma discharges [24, 29–32]. There is a clear need for time and space resolved diagnostic methods to understand the dynamics and properties of plasma chemistry instabilities [33, 34]. To date, the majority of

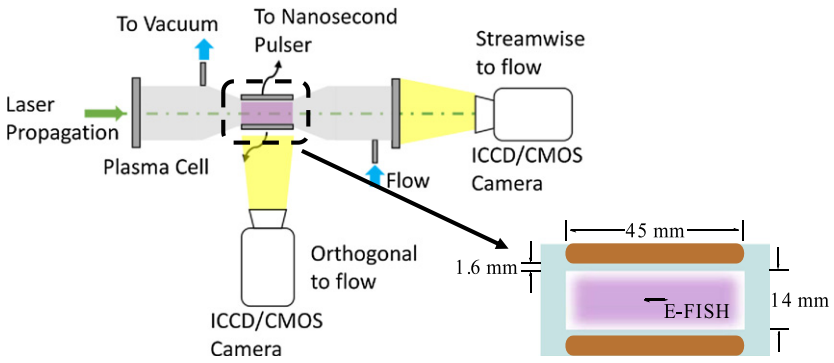

Figure 2. Experimental setup. Laser based diagnostics are setup in the direction of flow. Cameras are positioned either looking down the flow field (streamwise), or perpendicular to the flow (orthogonal). A schematic of the discharge with relevant dimensions is shown in the streamwise direction, along with the spatial position of the E-FISH diagnostic.

direct, transient electric field measurements have been limited to zero dimensional cases, representing a limitation on the use of the method for highly transient plasmas.

The goal of this paper is to explore this plasma thermal-chemical instability and probe key plasma properties to understand time evolution of its growth. This study will utilize recent *in situ* E-FISH measurement techniques to measure the spatially-averaged electric field (henceforth discussed as the 'measured electric field') measured across the femtosecond laser sheet along with ICCD images and Rayleigh scattering for plasma uniformity and temperature measurements. Using argon as a bath gas, with either methane, oxygen, or a methane/oxygen mixture added, the effect of these gas additions on the electric field and temperature profiles are measured. Broadband ICCD imaging is also recorded to explore the feedback effect of plasma filamentary constriction due to hydrocarbon oxidation. The results will show the distinct constriction and formation of non-uniform behavior solely due to the addition of hydrocarbon chemistry, as well as exploration into the parameter space and possible reasons for this phenomenon.

2. Experimental methods

The experimental apparatus, figure 2, has been reported previously for related experiments [35–37]. A rectangular quartz cell has been constructed with a plane-to-plane dielectric barrier discharge area of 44.5 × 44.5 mm square. The quartz has a dielectric constant of 3.78 and a thickness of 1.6 mm covering each metal electrode, with a quartz to quartz gap distance of 14 mm. Removable windows at the ends of the cell allows for coupling of various laser and imaging diagnostics in the direction of flow, while the quartz walls in the discharge region also allow for measurements in the direction perpendicular to the flow. All experiments maintained initial room temperature and a pressure of 50 Torr within the reactor. Total flow rates are 0.7 m s^{-1} for all conditions, with a plasma residence time of ~0.06 s. The fuel and oxygen mole fractions are held constant for all cases discussed below, with argon added to fill the remaining mole fraction if one of the mixture components is removed. Three cases are studied: a stoichiometric fuel/O_2 case (6.6% CH_4, 13.4% O_2, 80% Ar), a pyrolysis case (6.6% CH_4, 93.4% Ar) and a no fuel case (13.4% O_2, 86.6% Ar). A nanosecond-pulsed power supply (FID GmbH FPG 30-50MC4) is used for plasma generation, with a maximum repetition frequency of 30 kHz, FWHM of 12 ns, and maximum peak voltage of 32 kV (using both the positive and negative side of the supply), which is operated in a burst mode via an external digital pulse generator (SRS DG645). Representative current and voltage plots for this pulser can be seen in our previous works [36, 38]. A burst of 150 pulses at 30 kHz pulse repetition rate is used, with a total discharge time of 0.005 s for a single burst of pulses. The bursts are operated at 15 Hz, which allows for gas replenishment and to prevent coupling between bursts while minimizing data collection times.

Several diagnostics have been utilized in the present work. For imaging subsequent pulses within a single burst, simultaneous images of the plasma are taken using two PCO Dimax HD sCMOS cameras both in the streamwise as well as orthogonally to the direction of flow (see figure 2). Single shot images monitoring every pulse within a single burst are taken at 30 kHz with a gate of 1 μs for analysis of filament formation and growth within the given burst. For nanosecond resolution of the growth of a single pulse within the plasma burst, a CCD camera coupled to a LaVision PicoStar intensifier was used, with a gate of 1 ns, which provides time-dependent resolution into the pulse formation. Note that these images are not correlated for a single burst event. Thus, a total of 5 images were taken for each time point, for average comparison as well. These nanosecond images are only taken in the streamwise direction. Simultaneous voltage measurements are made using a Tektronix P6015A high voltage probe.

Electric field measurements are performed using the E-FISH generation method (E-FISH) [23, 24, 39–41]. The E-FISH setup in this experiment was similar to that used in our previous work [23, 24]. Briefly, a Spectra-Physics Solstice Ace femtosecond laser is used with a peak energy of ~7 mJ per pulse, centered at 800 nm and bandwidth of 15 nm, pulse duration of 60 fs, and a nominal beam diameter of 10 mm is used as the pump laser source. The beam is focused into the discharge region using an $f = 400$ mm cylindrical lens in the direction of gas flow. This creates a measurement volume of ~25 μm × 1 cm × 2 cm (beam waist × beam

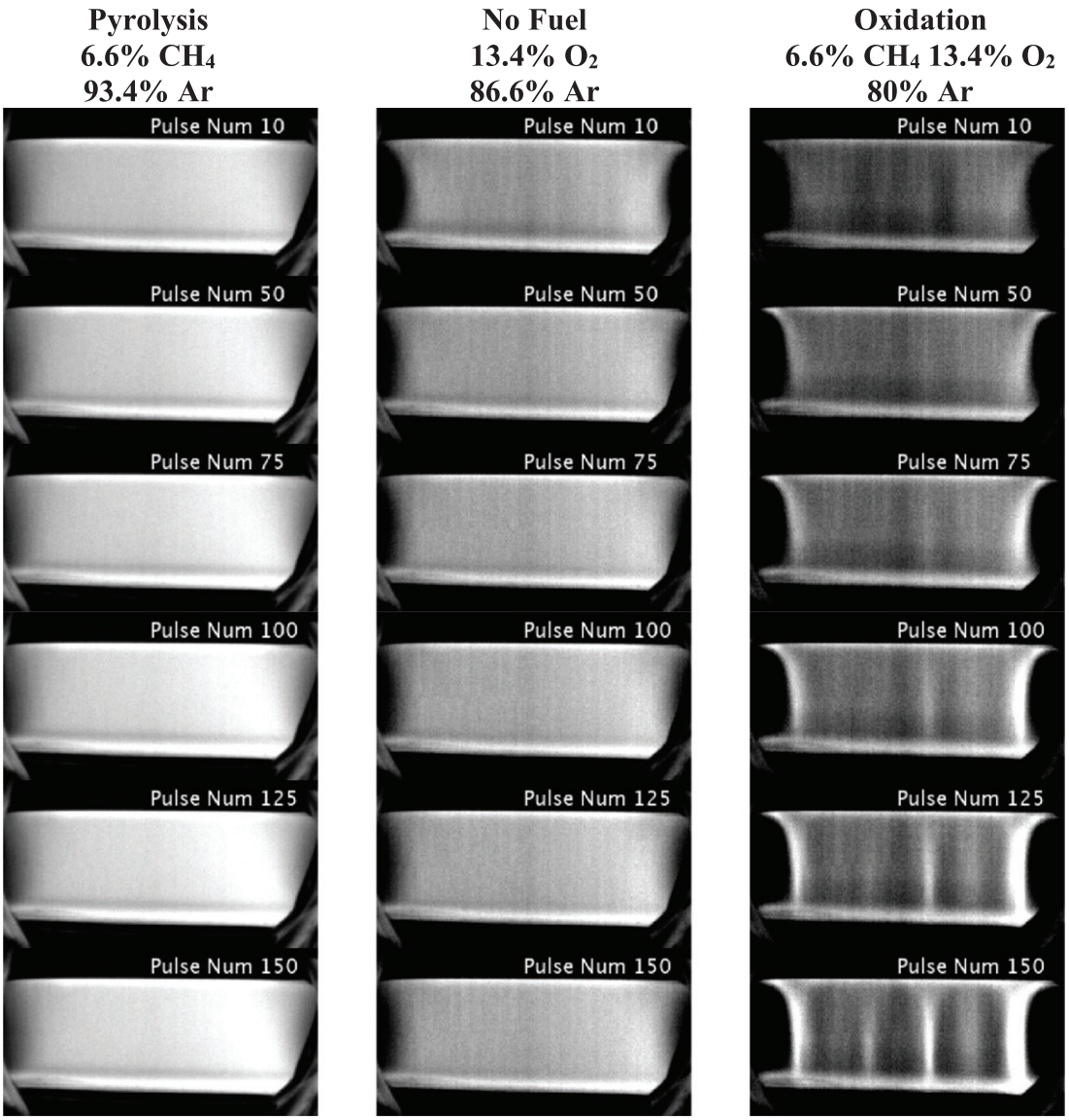

Figure 3. CMOS images of a single burst of the plasma discharge. The fuel and oxygen mole fractions are held constant (6.66% CH_4, 13.34% O_2) with argon added to fill the remaining mole fraction when a mixture component is removed. Intensities are not to scale, for the pyrolysis case and the no fuel cases, camera gain is reduced to prevent saturation.

diameter $\times$ confocal beam parameter). The second harmonic light is collimated using a matched cylindrical lens, and the pump and second harmonic light are then spectrally separated using a dispersion prism. The second harmonic signal beam is focused directly onto the photocathode of a PIMax4 1024i ICCD using a third, cylindrical lens allowing for 1D electric field imaging. Images are collected in a single shot fashion, and time-binning and averaging is completed in a post processing routine. Calibrations are taken in the same discharge cell using an AC power supply operated below the breakdown threshold, with the same gas mixtures as used in the discharge. For the 1D measurements, calibrations are obtained for each pixel with the minimum detectivity around 1 kV cm^{-1}.

Rayleigh scattering was performed in a setup previously used for Thomson scattering [37]. A Quantel Q-smart 850 Nd:YAG laser with pulse width of 6 ns and pulse energy of 380 mJ was focused into the center of the rectangular quartz cell described above. For centerline measurements, apertures were put in place to reduce the amount of stray light. Plasma emission was filtered by a 532 nm bandpass filter with full width at half maximum of $\pm$1 nm. The filtered light is then imaged onto a PIMAX 1300 ICCD with a 20 ns gate width. Through direct imaging, a 1D measurement along the laser propagation direction was captured with $\sim$100 μm resolution per pixel.

For the Rayleigh scattering, E-FISH and nanosecond resolved ICCD imaging, pulses 1–5, 10, 25, 50, 75, 100 and 150 were analyzed for the oxidative $CH_4/O_2/Ar$ case. Pulses 1, 2, 10, 50, 100, and 150 were measured for the CH_4/Ar, and O_2/Ar cases, as the plasma was uniform and showed no evidence of filament formation.

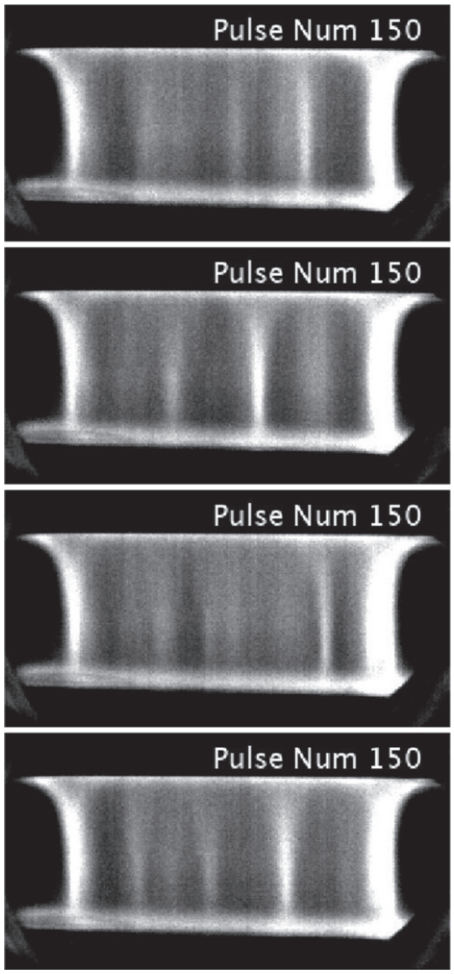

Figure 4. Snapshots of pulse 150 from various bursts in the streamwise direction. Filament location is seen to be moving from burst to burst.

3. Results and discussion

3.1. High speed imaging of the 150 pulse plasma burst

CMOS images (1 μs gate) of pulses 10, 50, 75, 100, 125 and 150 within a single burst of pulses along the axis of flow (streamwise) for each mixture are shown in figure 3. The cases of plasma discharge in the three different mixtures are compared to show qualitatively the effect of mixture composition and plasma assisted chemical reactions on plasma instability. Both the pyrolysis (6.6% CH_4, 93.4% Ar) and no fuel (13.4% O_2, 86.6% Ar) cases clearly have uniform discharges throughout the burst. There is a known difference in intensity here due to the change in the argon mole fraction, as well as the weakening of the discharge due to electron attachment reactions caused by the addition of oxygen to the plasma [12]. For the oxidative case (6.6% CH_4, 13.4% O_2, 80% Ar), however, where low temperature methane oxidation is initiated through plasma-assisted reaction pathways [36], filamentation is observed. This filamentation (instability) does not occur immediately, as there is still a diffuse discharge in early pulse numbers within the burst, but with increasing pulse numbers, the discharge grows increasingly filamentary. The transition to distinct filaments typically occurs between pulse 75 and 100. As seen in the videos presented in the supplementary materials (https://stacks.iop.org/PSST/29/105012/mmedia), these bright filaments are clearly due to constriction of the diffuse discharge into filamentary plasma channels, as the surrounding area grows gradually dimmer while the filament strengthens from pulse to pulse. Note that, as stated above, the intensity scaling for a given set of images is kept constant, so the observed dimming of the region between filaments is not an adjustment in scale. The filaments are consistent in a single burst from pulse to pulse: once formed in a particular location, they are stable until the burst ends and the gas is refreshed. This is consistent with previous filamentation work by Clevis *et al*, which also found residual pre-ionization effects from previous pulses within a single burst [9]. The filaments on the sides of the electrodes tend to be stronger, stable and reproducible across different bursts. Thus, we conclude that these are likely caused by plasma edge effects rather than a thermo-chemical instability. For the remainder of the discussion this work, these edge formations will not be discussed in order to focus on the center plasma filaments, as they are formed solely due to the plasma-combustion interaction rather than geometric factors. Therefore, the present experiment clearly suggests the existence of plasma thermal-chemical instability proposed in our previous study [22], which, as described above, used a one-dimensional numerical model for $H_2/O_2/N_2$ mixtures and found that chemical reactions affected the critical plasma current for transition between a homogeneous and contracted (filamentary) states. Endothermic electron impact fuel dissociation (the dominant pathway in pyrolysis) increased the plasma stability, while exothermic oxidation reactions lead to a quicker transition to the contracted state, even when the model artificially suppressed the additional heat release due to these reactions, suggesting that the composition change caused by these reactions plays a role in stability. The experimentally measured temperature of the discharges using Rayleigh scattering is discussed in section 3.4.

Figure 4 shows pulse 150 for the oxidative case, taken with the same camera conditions for four different bursts. It can be seen that aside from the edge effects, the filaments move in location from burst to burst as the gas replenishes, as predicted in the literature [12]. The strongest filament does seem to appear on the right side of the image more often, which may be due to slight deformities in the cell construction such as non-uniformities in the quartz or electrode gap distance. The random movement of the filament does confirm, however that these constrictions are due to a chemical coupling caused by the oxidation reactions, and not due to the geometry or irregularities of the cell itself, which are weak enough in this case to just preferentially determine a larger region where the strongest filament might form. Finally, to confirm the thermal coupling of this instability, an additional test was performed with 3000 pulse bursts (discussed in the supplemental figures S1 and S2), where it was found that the discharge returned to a more uniform state with increased burst counts, demonstrating

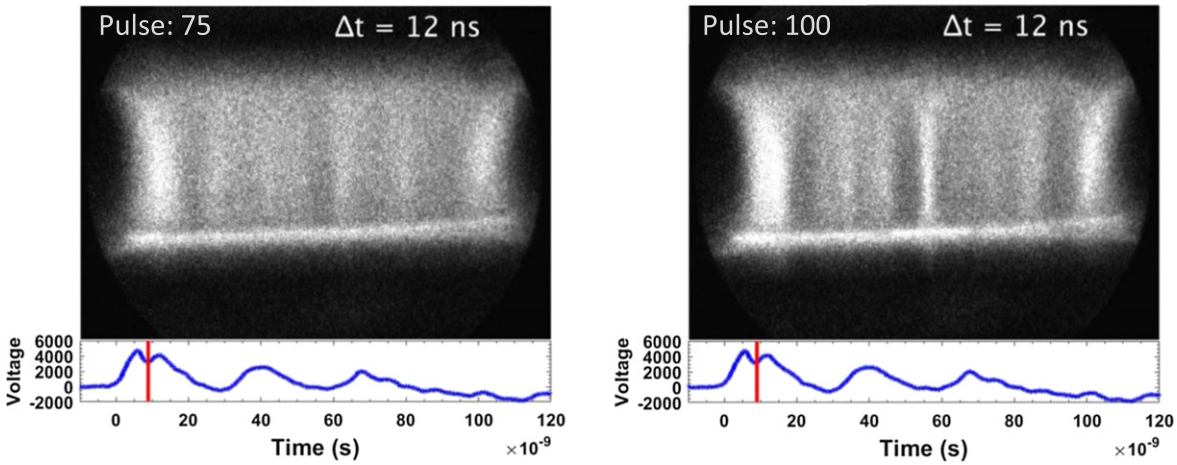

Figure 5. ICCD images (1 ns gate) of pulse 75 (left) vs pulse 100 (right) in the CH_4/O_2/Ar oxidative discharge case. Slight variation in intensity is seen at pulse 75, but significant filamentation is seen by pulse 100.

that the instability is strongly coupled to the local temperature and thermal conductivity of the mixture, as once enough time was provided for thermal diffusion within a burst the filamentation starts to homogenize.

3.2. Nanosecond resolved images of pulses within the 150 pulse burst

A 1 ns gate ICCD camera was used to image the formation and duration of these structures in a single pulse within the burst compared to the diffuse plasma. Ten images were taken at each time point, with a 1 ns step starting from 10 ns before the trigger pulse, out to 140 ns. Images in this case are still correlated in brightness, but each image is from its own individual burst. As stated above, voltage measurements were concurrently recorded for each pulse, along with the trigger for the camera, and is shown below the image, as can be seen in figure 5. Time $t = 0$ is set to 10% of the maximum voltage for waveform comparison, and to account for slight jitter in the inter-pulse timing, on the order of $\sim\pm5$ ns. A delay of 8 ns was added to the imaging data, accounting for internal processing and cable lengths, to correlate the initial emission from the plasma with the breakdown seen in the voltage waveform. The 1 ns time step between images is well known, due to the low jitter (<25 ps) of the pulse generator (SRS DG645). For this data set, all time points will be referenced from the determined zero point, as Δt values.

Figure 5 shows pulse 75 and pulse 100 for the oxidation case at the same time instant of $\Delta t = 12$ ns, with 1 ns ICCD gating. As is shown both in figure 3 and by the videos in the supplementary material, the plasma is uniform for early pulses and transitions to distinct filaments between pulse 75 and 100, as discussed previously. Further evidence is shown here, where with nanosecond resolution distinct filamentary structures are seen in pulse 100. Pulse 75 is starting to show non-uniformities in overall structure, especially compared to the no fuel and pyrolysis cases (see SI figures S3–S11), but the diffuse plasma nature is still present.

Figure 6 shows several time instances of pulse 150 for the methane oxidation case, again with 1 ns time-resolution gating. At this point the plasma is completely nonuniform, with initial emission seen when Δt is 9 ns. Compared to the previous data for pulse 100 in figure 7 at $\Delta t = 12$ ns, the emission is seen to be drastically more filamentary in nature. By $\Delta t =$ 12 ns in this case, the plasma is fully established, with the individual filaments connecting at the top and bottom. As the voltage drops, the emission begins to decrease through $\Delta t = 16$ ns, with only faint emission seen at the strongest channels for $\Delta t = 20$ ns. By 26 ns, only faint emission is seen at the top and bottom, likely due to residual surface charge, and afterglow in several of the channels. These images reveal that the filaments dominate the discharge structure at this point, with the blurring effect seen in the earlier 10 μs images due to the longer imaging time. Further 1 ns time-resolved images can be seen in the supplementary material figures S3–S11 for pulses 10, 50, and 150 for the pyrolysis and no fuel cases, and pulses 10, 50 and 100 for the oxidative case. This further emphasises the distinctly different filamentary discharge mode observed in the oxidative case, where some variation in the discharge is visible as early as pulse 10 progressing through pulse 100 to true filaments, while comparatively very little observable difference is found in any of the pyrolysis or no fuel pulses. Between pulse 100 and 150, then, we see a regime change from beginnings of filaments to full constriction and an entirely non-uniform discharge structure. Overall emission seems to follow well with the voltage waveform, with an approximate duration of $\sim$10–15 ns. This is slightly longer in the pyrolysis case, as the additional argon mole fraction seems to extend the relaxation time compared to the no fuel and oxidative cases. The secondary voltage pulses seen in the waveform data do not seem to result in significant emission, suggesting that these secondary pulses, still with significant voltage applied, do not result in volumetric breakdown and subsequent emission. As will be discussed later, however, these voltage pulses still show some electric field present in the plasma, so may be sub-breakdown energy deposition at lower E/N values and could still play a role in the chemical kinetics through vibrational pumping.

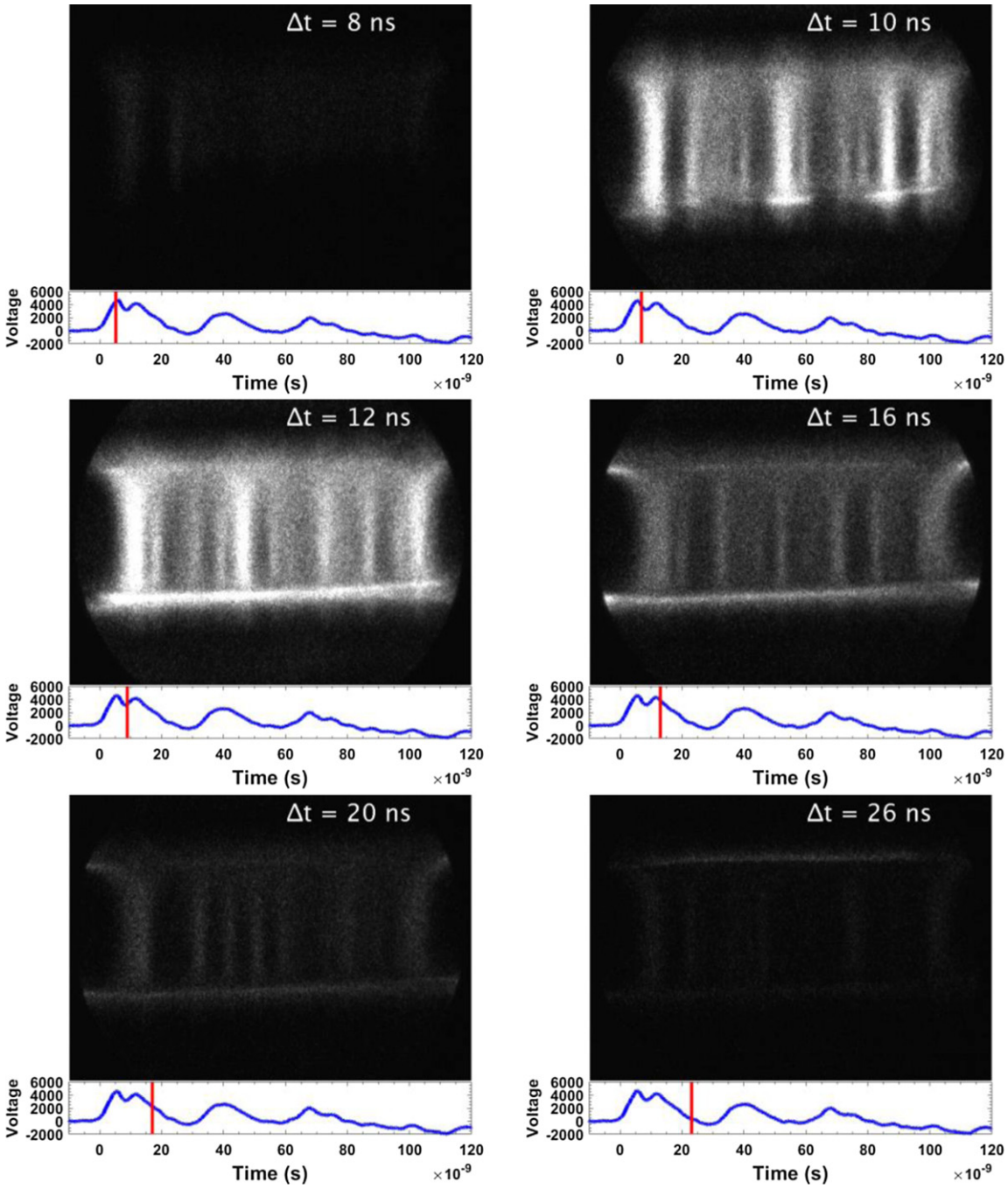

Figure 6. Nanosecond-resolved ICCD image of pulse 150 at various time steps in the CH_4/O_2/Ar oxidative discharge case. The discharge in this case starts filamentary, and lasts around 12 ns, with some emission at the surface of the dielectric persisting slightly longer.

3.3. Measurements of changes in measured electric field using E-FISH

The time-dependent electric field during the nanosecond pulses was measured using the E-FISH method. Spatially averaged calibrated E-FISH measurements for pulses 10, 100, and 150 are shown as the red points in figure 7 for the 3 discharge cases (i.e. pyrolysis, no fuel, and oxidation). Additionally, the concurrently measured applied voltage to gap ratio waveforms are shown as the blue lines (including the thickness of both dielectric barriers). The E-FISH results demonstrate the absolute value of the spatially averaged electric field across the 1D measurement region *within* the discharge while the applied voltage to gap ratio is presented to demonstrate the voltage *supplied* to the discharge. Note that the differences between these two curves are due largely to sheath formation, surface charges upon the dielectric, as well as the conductivity of the plasma.

For the CH_4/Ar discharge (left column of figure 7), the strongest of the 3 discharges and which the plasma imaging confirmed to be diffuse, there is good agreement with the initial high voltage rise, followed by a sharp reduction in the electric field offset from the applied voltage. This is

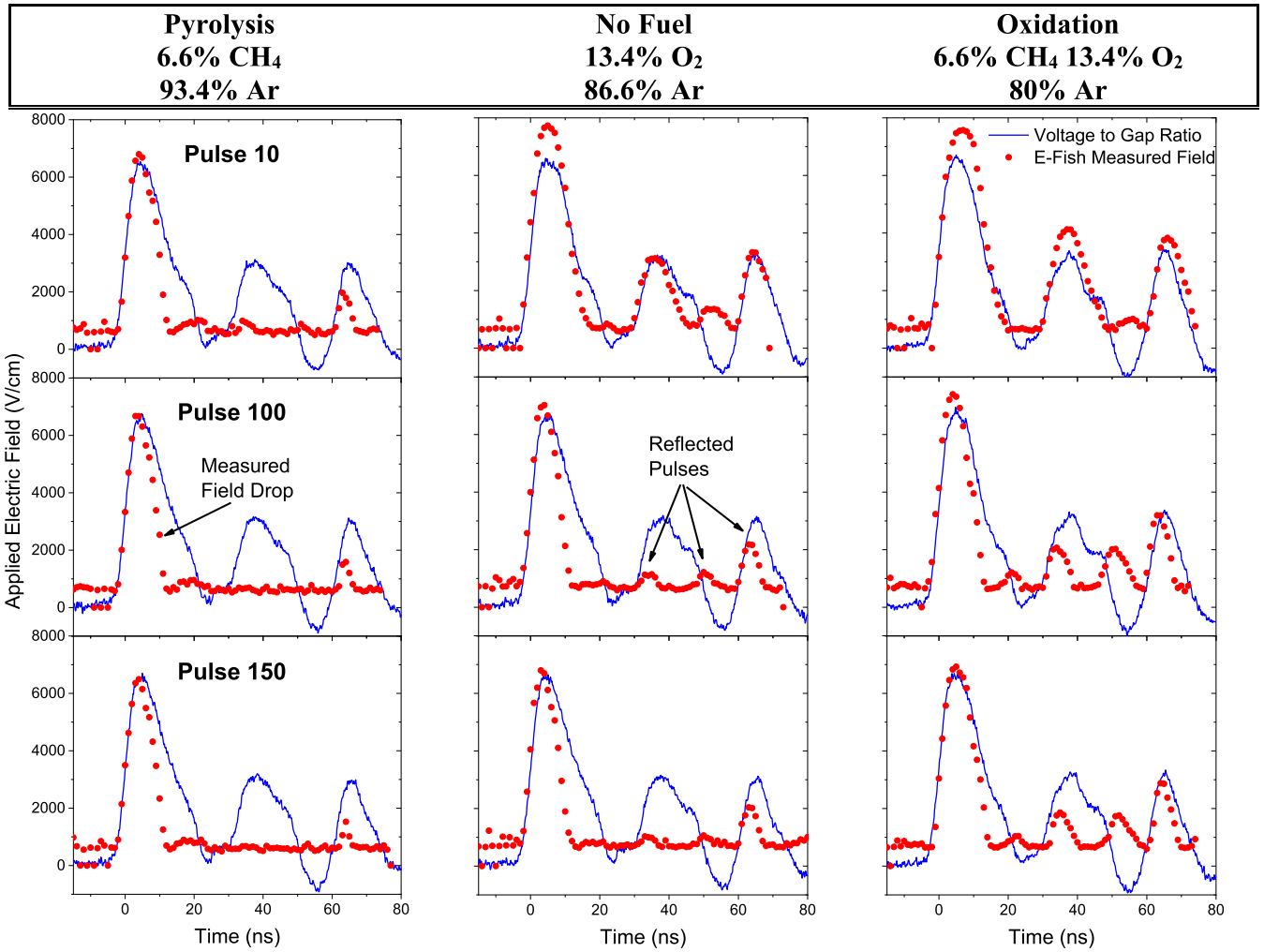

Figure 7. E-FISH data from pulses 10, 100 and 150 for the pyrolysis, no fuel, and oxidation cases of the plasma discharge. The dotted red points are the electric field as measured by E-FISH, while the blue solid lines are the voltage to gap ratio, including the thickness of both dielectric barriers, measured using a Tektronix P6015A high voltage probe. The pyrolysis plasma is the strongest, with the most argon, and dampens out the field effects of the later pulses due to a strong sheath. Oxygen acts as an electron scavenger, which allows for field effects to be felt in the bulk plasma in the other two cases.

consistent with a breakdown event, where the drop is due to the gas mixture ionizing and becoming conductive. Following the volumetric breakdown, the field in the plasma is seen to remain nearly zero, indicating the presence of a stable, diffuse plasma across the laser sheet. It is important to note E-FISH measurements under an open load without breakdown confirmed that the additional pulses seen after the main pulse in the high voltage waveform (t = 25–80 ns) are an actual voltage applied across the gap due to the pulser supplying secondary pulses. While the third and final 'secondary' pulses exhibits a small increase in the field, the preceding pulse of similar amplitude demonstrates nearly zero field, limited by the 1 kV cm^{-1} detection limit of the experimental setup. Once again, this is consistent with a diffuse discharge, where the highly mobile electrons are able to react to the applied voltage to negate the field within the discharge gap. The field rise and sharp drop observed in the final pulse could be due either to a reduction in the electron number density (due to recombination and electron attachment to CH_4) or may represent a possible field reversal as the E-FISH method is sensitive to E^2 and thus cannot determine positive or negative fields. Time gated, ICCD imaging does reveal a faint emission during some bursts corresponding with this second rise, indicating secondary breakdown can occur with strong enough field.

The middle plot shown in figure 7 is the electric field development for the O_2/Ar case. While the results are similar to the CH_4/Ar data, the smaller secondary pulses seen in the high voltage waveform consistently have a larger accompanying field, likely due to lower electron density than the pyrolysis case. Due to attachment, the O_2 addition scavenges electrons quickly, reducing the plasma density. At the later times, there are not enough electrons to fully shield the secondary pulses, allowing for the stronger electric field present. Finally, the right plots shown in figure 7 demonstrate the oxidation case. Here, it can be seen that the initial pulses have much weaker shielding, and the field in earlier pulses follows the voltage waveform. While there is still an absolute offset between the E-FISH and voltage to gap ratios, these

secondary pulses are very active even through pulse 150. From the E-FISH measurements, it is clear that oxidation chemistry is scavenging electrons or causing a surface charge imbalance. It is important to note that with secondary field, there is also additional energy deposition in the bulk plasma, as lower *E*/*N* values will pump vibrational modes, which could possibly extend or enhance oxidation kinetics. While our previous 1D modelling work on hydrogen plasmas [22] suggests that electron-chemical interactions can cause or inhibit the formation of these filaments, work is still ongoing with a methane model incorporating higher strength *E*/*N* fields to demonstrate this and will be presented in a future paper. From 0D modelling with helium [36, 42, 43], the reactions most responsible for this low temperature heat release were O, O(^{1}D) and OH reactions with CH_4. As these reactions cannot be activated in either no fuel or pyrolysis case, it is possible that either the heat release from these reactions, or the formation of local concentrations of reactive radicals leads to this filamentation behavior. Work looking into which reaction pathways are most responsible for the thermal-chemical instability is ongoing.

The results presented above demonstrate the time and space averaged electric field measured across the femtosecond laser sheet. In order to further elucidate the effect of oxidation chemistry, we attempt to resolve the electric field with 1D spatial accuracy across the ~5 mm width in the center of the plasma, as seen in figure 2. Unfortunately, shot-to-shot uncertainty in the E-FISH experiment does not allow for absolute single shot measurements as a satisfactory signal to noise requires significant build-up of shots. For this reason, the relative single shot E-FISH profile at $t = 3$ ns on pulse 140 is shown in figure 8. The profile has been normalized to the average signal count across the laser sheet. Some evidence for increased electric fields may be seen in the raw signal count data. In figure 8, the different colors represent single shot measured values, with the mean given by the thicker black line. The individual spikes appear to be regions with significantly higher measured electric fields as the E-FISH signal follows the square of the local field. Even still, there are several caveats to this. First, these spikes are also seen in the methane and oxygen datasets, albeit at much lower (3–4x) relative intensities and frequency of occurrence. It is possible these are real signals, in which case there is also fluctuation in the electric field in the other two cases, which would need to be explored further. Second, the electric field measurement is inherently spatially averaging along the laser path, as it generates signal along the entirety of the beam confocal parameter ($L_c \sim 2$ cm). For the current experiment, this entire range is within the plasma discharge region by design, but this makes it difficult to study the apparent spikes that may be present due to these filaments. While it is clear for the plasma as a whole that chemistry is changing the plasma parameters, further study is certainly required with a spatially stationary filament to determine whether these electric field spikes are due to the onset of filamentation or another, currently confounded parameter. To what extent the combustion oxidation is in turn affecting the localized electric field through a feedback loop is still an open question.

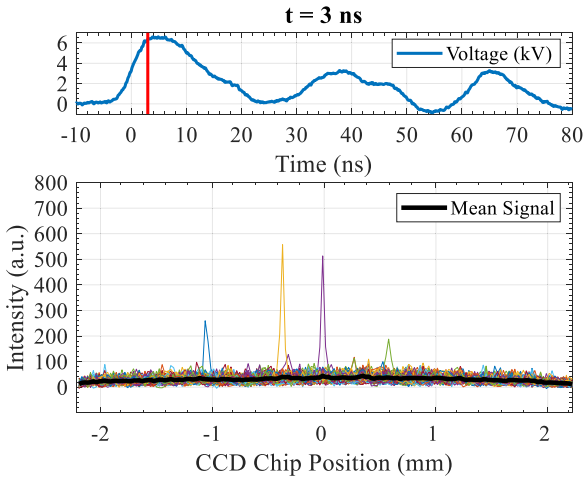

Figure 8. Multiple 1D single shot E-FISH intensity counts and corresponding location in the voltage time-dependent waveform for pulse 140, 3 nanoseconds after the start of electric field rise. Mean signal is shown by the thick black line.

3.4. Rayleigh scattering measurements to determine number density

Finally, measurements of the bulk gas number density were taken to look at the heating in the plasma. In general, some gas heating is expected due to Joule heating from the discharge. Previous studies [35–37] have demonstrated that oxidation chemistry clearly contributes to the bulk gas heating during the plasma burst, with up to 50% higher temperature rise in the oxidation case compared to an oxygen or pyrolysis plasma. Figure 9 shows the number density in the plasma as a function of pulse number for the $CH_4/O_2/Ar$ oxidation case. Assuming an ideal gas is maintained, this results in the temperature rise seen by the right-axis temperature scale. The error bars were calculated using a 5% uncertainty in the laser pulse energy which directly translates to uncertainty in the measured Rayleigh image intensity. Lefkowitz *et al* found a temperature rise to ~330 K after 150 pulses in a stoichiometric CH_4/O_2/He mixture with 75% helium dilution [36]. It would be expected to see a higher temperature rise in the argon case due to the much lower thermal diffusivity of argon compared to helium. Even with the error bars due to the uncertainty of the measurement, there is a clear temperature rise, consistent with the previously published results, throughout the burst [36, 37]. This bulk temperature rise is too low to fully dampen the instability formation. As previous data has shown the temperature rise for argon plasmas similar to this to be roughly linear, extrapolation out to 1500 pulses reinforces the earlier discussion that bulk heating helped remove the instabilities at longer pulse numbers [35, 38]. The much higher temperature from longer bursts provides an increase in mass diffusion, and also makes the local disturbance a smaller fraction of the overall temperature, resulting in a more uniform plasma.

Rayleigh scattering is also capable of 1D spatially resolved measurements, but along the flow direction of the discharge region, opposite the direction of the E-FISH measurement. As seen from the images in the supplement figures S1 and S2,

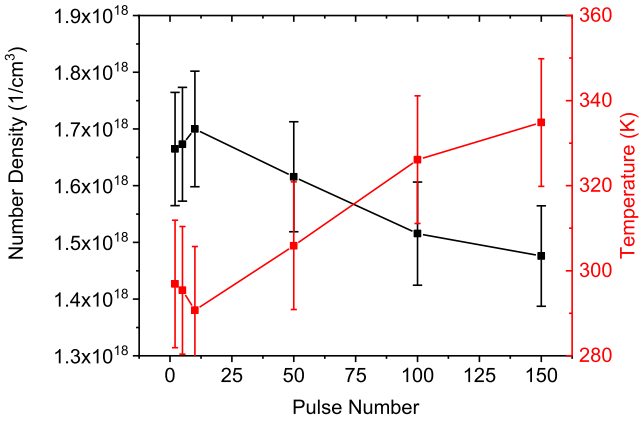

Figure 9. Bulk number density (left axis) and corresponding ideal-gas temperature (right axis) as a function of pulse number for the 150 pulse burst in the $CH_4/O_2/Ar$ case. Data has been averaged over 100 shots. The error was determined by using 5% as the uncertainty in the laser pulse energy.

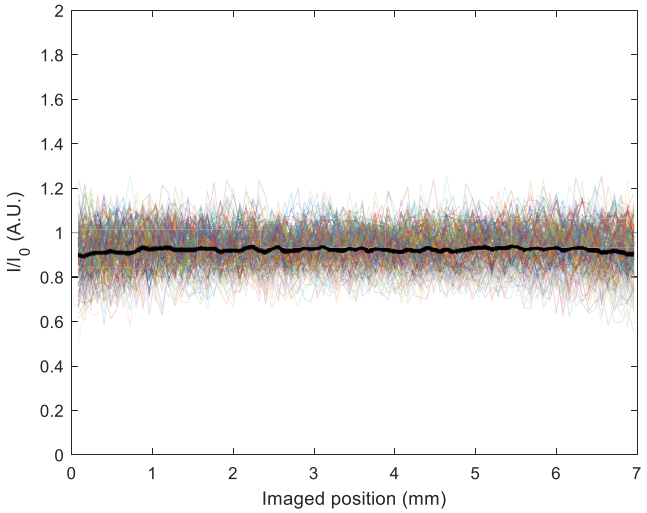

Figure 10. Raw 1D Rayleigh signal as a function of pixels for pulse 100 in the $CH_4/O_2/Ar$ case. No spatial peaks are observed suggesting a local rise in temperature due to filament formation.

however, these filaments are appearing in both spatial directions, so similar to the E-FISH, fluctuations of temperature should be visible. No large fluctuations of number density were seen for the present conditions, however. To ensure laser overlap with the filaments, a series of measurements were taken, both spatially at 1 mm steps across a 1 cm range as well as temporally, at 1 ns increments (note that the laser pulse duration was 8 ns), for pulse 150 of the oxidation case, where the filaments were seen to be the most severe. When averaged, all of the Rayleigh data falls within the error bars for pulse 150 in figure 9. A subset of the raw data, presented as a fraction of the signal I to the background data I_o can be seen in figure 10, with the average measurement in black. While there is significant noise in this data (as represented by the error bars in figure 9), no large spikes are seen for any given run, such as was observed in the single shot E-FISH results (see figure 8). There are two primary sources of uncertainty that could explain the apparent lack of temperature rise in the Rayleigh scattering data. First, the experiment may lack enough spatial resolution to accurately capture the filaments. It has been demonstrated in the literature that these channels can be extremely narrow, on the order of 100–200 μm [14, 22]. The current spatial resolution is on the order of 100 μm per pixel, which could be smearing any observed temperature changes. Secondly, if this is the case, it is also possible the laser is never directly interacting with the filament. A possible explanation, then, is that the actual temperature fluctuation is the same or smaller order than our error bars, which would result in a local variation in temperature of less than approximately $\pm$20 K. This hypothesis would suggest that the oxidation chemistry is playing a larger role for the formation of these filaments than the thermal instability, as this deviation is much smaller than the 10%–20% listed in the literature [44, 45]. Again, subsequent experiments are required to fully explain this measurement, but it seems plausible that the local heating effect is small, as the measurements do still capture the average temperature rise across the burst quite well. If this is true, it would mean the oxidation chemistry is playing a role in the formation of preferential ionization channels by changing the gas composition through intermediates and product species.

4. Conclusion

The effects of plasma-assisted low temperature fuel oxidation and pyrolysis on the formation of plasma instability and electric field distribution is explored for a nanosecond repetitively pulsed plasma discharge using spatial and time-resolved diagnostics. The results show clearly that an oxygen/methane stoichiometric mixture with an argon bath gas resulted in significant filamentation formation in the plasma during a burst of nanosecond pulses. On the other hand, discharges of oxygen/argon and methane argon result in a uniform discharge without any evidence of streamer formation. This result demonstrated that plasma assisted low temperature oxidation of methane promoted the formation of plasma thermal-chemical instability. These filaments travel with the bath gas but at a reduced velocity, suggesting that the formation is tied to changes in ionization potential of species formed during the oxidation process. This order of magnitude change is likely due to the slower thermal conductivity of argon: previous helium data in reference [36] calculates the thermal conductivity of He to be about an order of magnitude higher than argon, which is why no evidence of filamentation is found in their oxidation data, even up to 30 kHz continuous pulsing. Averaged electric field measurements show changes in the secondary pulses and secondary discharge formation, but little change in the primary breakdown event. Single shot raw data counts suggest there may be greatly increased localized electric fields present on the order of $\sim$100 μm's, but further experimentation is required to verify these results. Rayleigh scattering is utilized to study the bulk number density, and accurately captures the average temperature rise during the discharge. The Rayleigh scattering data shows no evidence of increased temperature in the

filaments, suggesting either extremely small filamentary structures or the importance of local chemistry in the instability formation.

Acknowledgments

The authors would like to thank ExxonMobil for providing funding for this research area through its membership in the Princeton E-filliates Partnership of the Andlinger Center for Energy and the Environment. ACR and YJ are grateful to the U.S. Department of Defense for their funding through the National Defense Science & Engineering Graduate (NDSEG) Fellowship program, Princeton SEAS innovation fund and the Andlinger Center for Energy and the Environment (ACEE) Grant, DOE-NETL UCFER Grant, the DOE Plasma Science Center grant DE-SC0020233, and NSF Grant CBET 1903362. ACR, YJ and TYC are also grateful for the NSF-EFRI DCheM award: Engineering Interfaces between Plasma, Catalysts, and Reactor Design for Natural Gas Conversion to Liquid Products. TYC was partially supported through the Program in Plasma Science and Technology at Princeton University Fellowship.

ORCID iDs

Aric C Rousso https://orcid.org/0000-0002-5710-3233
Timothy Y Chen https://orcid.org/0000-0003-3026-9767
Shuqun Wu https://orcid.org/0000-0002-5519-8099

References

[1] Mehta P, Barboun P, Herrera F A, Kim J, Rumbach P, Go D B, Hicks J C and Schneider W F 2018 *Nat. Catal.* **1** 269–75
[2] Vach H and Brulin Q 2005 *Phys. Rev. Lett.* **95** 165502
[3] Yang X, Zhao F, Yeh Y-W, Selinsky R S, Chen Z *et al* 2019 *Nat. Commun.* **10** 1543
[4] Zhao X, Liu Y, Inoue S, Suzuki T, Jones R O *et al* 2004 *Phys. Rev. Lett.* **92** 125502
[5] Pai D Z, Lacoste D A and Laux C O 2010 *J. Appl. Phys.* **107** 093303
[6] Simeni Simeni M, Tang Y, Hung Y-C, Eckert Z, Frederickson K and Adamovich I V 2018 *Combust. Flame* **197** 254–64
[7] Tang Y, Simeni M J S, Yao Q, Frederickson K and Adamovich I V 2019 *AIAA Scitech 2019 Forum* (American Institute of Aeronautics and Astronautics)
[8] Liu C, Dobrynin D and Fridman A 2014 *J. Phys. D: Appl. Phys.* **47** 252003
[9] Clevis T T J, Nijdam S and Ebert U 2012 *J. Phys. D: Appl. Phys.* **46** 045202
[10] Griskey M C and Stenzel R L 1999 *Phys. Rev. Lett.* **82** 556–9
[11] Lashinsky H 1964 *Phys. Rev. Lett.* **12** 121–3
[12] Raizer Y P 1991 *Gas Discharge Physics* (Berlin: Springer)
[13] Golubovskii Y B, Nekuchaev V, Gorchakov S and Uhrlandt D 2011 *Plasma Sources Sci. Technol.* **20** 053002
[14] Shneider M N, Mokrov M S and Milikh G M 2014 *Phys. Plasmas* **21** 032122
[15] Shneider M N, Mokrov M S and Milikh G M 2012 *Phys. Plasmas* **19** 033512
[16] Ju Y and Sun W 2015 *Prog. Energy Combust. Sci.* **48** 21–83
[17] Ju Y, Reuter C B, Yehia O R, Farouk T I and Won S H 2019 *Prog. Energy Combust. Sci.* **75** 100787
[18] Adamovich I V, Nishihara M, Choi I, Uddi M and Lempert W R 2009 *Phys. Plasmas* **16** 113505
[19] Yin Z 2013 Fuel Oxidation and Ignition by Nanosecond Pulse Discharges at Elevated Temperatures *PhD Dissertation* (The Ohio State University) https://etd.ohiolink.edu/pg_10?0::NO:10:P10_ACCESSION_NUM:osu1373812880
[20] Choi I, Uddi M, Jiang N, Adamovich I and Lempert W 2009 *47th AIAA Aerospace Sciences Meeting Including the New Horizons Forum and Aerospace Exposition* vol 0 (American Institute of Aeronautics and Astronautics)
[21] Lanier S, Bowman S, Burnette D, Adamovich I V and Lempert W R 2014 *J. Phys. D: Appl. Phys.* **47** 445204
[22] Zhong H, Shneider M N, Mokrov M S and Ju Y 2019 *J. Phys. D: Appl. Phys.* **52** 484001
[23] Dogariu A, Goldberg B M, O'Byrne S and Miles R B 2017 *Phys. Rev. Appl.* **7** 024024
[24] Goldberg B M, Chng T L, Dogariu A and Miles R B 2018 *Appl. Phys. Lett.* **112** 064102
[25] Adamovich I V, Butterworth T, Orriere T, Pai D Z, Lacoste D A and Cha M S 2020 *J. Phys. D: Appl. Phys.* **53** 145201
[26] Chng T L, Naphade M, Goldberg B M, Adamovich I V and Starikovskaia S M 2020 *Opt. Lett.* **45** 1942–5
[27] Finn R S and Ward J F 1971 *Phys. Rev. Lett.* **26** 285–9
[28] Sitz P and Yaris R 1968 *J. Chem. Phys.* **49** 3546–57
[29] Retter J E and Elliott G S 2019 *Appl. Opt.* **58** 2557–66
[30] Cui Y, Zhuang C and Zeng R 2019 *Appl. Phys. Lett.* **115** 244101
[31] Tang Y, Simeni Simeni M, Frederickson K, Yao Q and Adamovich I V 2019 *Combust. Flame* **206** 239–48
[32] Chng T L, Orel I S, Starikovskaia S M and Adamovich I V 2019 *Plasma Sources Sci. Technol.* **28** 045004
[33] Goldberg B M, Reuter S, Dogariu A and Miles R B 2019 *Opt. Lett.* **44** 3853–6
[34] Orr K, Tang Y, Simeni Simeni M, van den Bekerom D and Adamovich I V 2020 *Plasma Sources Sci. Technol.* **29** 035019
[35] Rousso A, Mao X, Chen Q and Ju Y 2019 *Proc. Combust. Inst.* **37** 5595–603
[36] Lefkowitz J K, Guo P, Rousso A C and Ju Y 2015 *Phil. Trans. R. Soc.* A **373** 20140333
[37] Chen T Y, Rousso A C, Wu S, Goldberg B M, van der Meiden H, Ju Y and Kolemen E 2019 *J. Phys. D: Appl. Phys.* **52** 18LT02
[38] Rousso A, Yang S, Lefkowitz J, Sun W and Ju Y 2017 *Proc. Combust. Inst.* **36** 4105–12
[39] Goldberg B M, Reuter S, Dogariu A and Miles R 2019 *AIAA Scitech 2019 Forum* vol 0 (American Institute of Aeronautics and Astronautics)
[40] Simeni M S, Goldberg B, Gulko I, Frederickson K and Adamovich I V 2017 *J. Phys. D: Appl. Phys.* **51** 01LT01
[41] Simeni Simeni M, Goldberg B M, Zhang C, Frederickson K, Lempert W R and Adamovich I V 2017 *J. Phys. D: Appl. Phys.* **50** 184002
[42] Mao X, Rousso A, Chen Q and Ju Y 2019 *Proc. Combust. Inst.* **37** 5545–52
[43] Chen Q, Yang X, Sun J, Zhang X, Mao X, Ju Y and Koel B E 2017 *Plasma Chem. Plasma Process.* **37** 1551–71
[44] Fridman A 2008 *Plasma Chemistry* (Cambridge: Cambridge University Press)
[45] Fridman A, Chirokov A and Gutsol A 2005 *J. Phys. D: Appl. Phys.* **38** R1–24